RESEARCH ARTICLE

mm-Wave Metasurface Unit Cells Achieving Millisecond Response Through Polymer Network Liquid Crystals

ROBERT GUIRADO , **GERARDO PEREZ-PALOMINO** , **MANUEL CAÑO-GARCÍA,**
MORTEN A. GEDAY , **AND EDUARDO CARRASCO** , **(Senior Member, IEEE)**
Group of Applied Electromagnetism (GEA), Centre of Advanced Materials and Devices for Information and Communications Technology (CEMDATIC), ETSI
Telecomunicación, Universidad Politécnica de Madrid, 28040 Madrid, Spain

Corresponding author: Robert Guirado (r.guirado@upm.es)

ABSTRACT The slow response time of planar Liquid Crystal (LC)-based phase-shift metasurface and Reconfigurable Intelligent Surfaces (RIS) cells is addressed in this paper by introducing a polymer network LC (PNLC) mixture suitable at mm-wave bands. Since the conventional effective isotropic model used in optical cells for describing the PNLC is not suitable in RF, an effective anisotropic and uniaxial model for such mixture is provided and experimentally validated at 100 GHz for the first time. In order to compare the temporal performance and tunability of the PNLC, transmissive and reflective cells, containing conventional LC and PNLC, have been manufactured and measured at optical and mm-wave frequencies. The temporal responses of PNLC are also compared for both RF and optical cells, obtaining relevant differences between their improvement factors, which are also discussed. Specifically, a 50 fold response time improvement is attained in cells designed to work at 100 GHz, although at the expense of a 3X tunability reduction. The model, which is robust to varying angle of incidence and cell dimensions, has been experimentally validated by designing and manufacturing a PNLC reflectarray cell of a different geometry. The cell shows reconfigurability times of 210ms, representing a significant improvement with respect to state-of-the-art response time in mm-wave cells, which are in the order of several seconds.

INDEX TERMS Uniaxial model, metasurface, polymer network liquid crystals, reflectarray, RIS, mm-wave.

I. INTRODUCTION

Electronically reconfigurable metasurfaces are expected to be within the next trends in wireless communications. In the case of phase-shifting reflecting surfaces such as reflectarrays or Reconfigurable Intelligent Surfaces (RIS) [1], [2], [3], [4], their operating principle is based on dynamically modifying the spatial phase distribution of an incident electromagnetic wave, in order to obtain a reflected field that radiates a desired pattern [5], [6], [7]. This is done dynamically by

The associate editor coordinating the review of this manuscript and approving it for publication was Tutku Karacolak .

introducing specific phase shifts in the different unit cells that compose the surface, employing one of many different technologies [8]. Amongst them, lumped elements such as PIN diodes or varactors have been intensively used due to their fast switching capabilities [9], as well as RF MEMS [10] and graphene conductivity tuning [11]. However, these mechanisms either do not work at higher frequencies at a reasonable cost or are still quite immature. On contrary, Liquid Crystal (LC) is a well-developed technology with a large and established manufacturing industry, especially in optics. LCs can be used to provide electronically tunable local phase-shifting capabilities to each unit cell or pixel of a metasurface by

varying the pixel electrical permittivity [12], [13]. Applying a biasing electric field to any given pixel with a LC cavity makes its anisotropic molecules rotate, which results in a variation of their macroscopic effective dielectric properties.

The major advantage of LC lies in its low cost and ease of implementation in electrically large devices. Since all the pixels share the same LC cavity, the entire surface can be filled in a single-step process during the manufacturing stage, as opposed to lumped elements. Besides, the power consumption of this technology is close to zero, as biasing the pixels requires a certain voltage but there is very low current flow. Their operating frequency range is wide (DC to visible), thus allowing for tunable metasurfaces in mm and sub-mm wave frequencies. Although LC-based resonant devices at low GHz bands have been implemented, the true potential of this technology lies in the higher frequencies (100 GHz and above), contrary to other technologies in which increasing the frequency worsens their applicability. However, the thick cavity structures ($\sim 100\mu m$) required in mm-wave devices lead to slow response times of the LC molecules, currently in the order of seconds [14], [15]. In RF LC based devices the achievable phase range is limited by the variation in LC permittivity and electromagnetic resonances are needed to increase it. This, in turn, adds losses, which limits the minimum thickness of the LC cavities. In conventional LCs, that is, pure nematic uniaxial LC materials that have not been mixed or altered, their molecules respond in micro to milliseconds to an externally applied electric field excitation, hereby the molecule rise time may be reduced using overdrive techniques in the bias signals [16], [17]. However, the LC relaxation response, when the excitation is removed, is governed exclusively by the material elastic constants and surface anchoring and not by an external driving force. Consequently, thick LC cavities lead to increased relaxation times, which becomes the limiting factor in the device dynamics. To dynamically reconfigure an LC-based reflecting surface requires updating the bias voltages in all the cells of the array. Therefore, rapid responses to both voltage increase (excitation) and decrease (relaxation) are needed as the global temporal response of the array will be given by the slowest transition. In RIS, for instance, this can be a problem for applications requiring fast reconfigurability (e.g. high-mobility scenarios or tracking [18]).

Different solutions have been proposed to overcome this limitation, although none of them has been successfully implemented in mm-wave. For instance, by using dual frequency LCs, the LC molecules can be actively forced to rotate in both directions depending on the bias frequency, which allows controlling the relaxation times through the applied electric field [19]. Alternatively, polymer network LC (PNLC) mixtures achieve better time response, which is the focus of this work.

In PNLCs, a conventional LC is doped with a monomer, which upon polymerization yields a three-dimensional network that anchors the LC molecules in volume [20], [21], [22]. This network subdivides the entire LC cavity into domains, and since the anchoring energy of the molecules is much stronger in these small domains, the relaxation time is greatly reduced. However, the polymer network leads to a higher required excitation field and a reduced range of the effective LC permittivity, which in practice implies a reduction of the achievable phase range. The unknown properties of many LC materials in the mm-wave regime, together with the difficulty of obtaining a proper electromagnetic model of the complex PNLC molecules that allows designing and achieving reasonable phase ranges, are some of the challenges that has made this strategy go unconsidered in RF beyond few GHz, although it is known to work well in optics [23], [24], [25], [26]. Some works reported its usage in low-frequency transmission line phase shifters [27], [28], but without providing an electromagnetic model of the mixture that enables further design optimization. Although a PNLC model based on effective scalar permittivities (isotropic model) is used in optic ranges, it is not suitable in resonant structures, where the electromagnetic fields are more complex, and a more sophisticated model is needed to include the boundary conditions imposed by the device. In [17] and [29], an uniaxial model was demonstrated to be appropriated to accurately describe both steady and dynamic models, for conventional LC mm-wave metasurfaces and biasing sequences. However, these models can not be applied to PNLCs, as their molecules are not really uniaxial (sometimes could be assumed as biaxial) and the elastic constants of the new mixture are unknown. Currently no model of PNLC mixtures allows for predicting the response of resonant devices, and consequently, an accurate design of a device to meet specifications in mm-wave bands is not possible.

In this paper, a PNLC mixture which allows for the polymerization of the LC polymer dopant and works at 100 GHz is presented. This mixture has not been introduced before and is the first of its kind to show operability in mm-wave bands. Together with the mixture, a PNLC effective permittivity model for planar phase-shifting metasurfaces is obtained, enabling the design of devices with relaxation times reduced orders of magnitude with respect to using a conventional LC. It is shown for the first time that an uniaxial model can be used to emulate the complex behaviour of PNLCs in multi-resonant cells with enough accuracy, only by considering effective values of dielectric anisotropy. The model should be obtained from measurements for each PNLC mixture, dopant concentration, cell geometry and angle of incidence, as it tries to describe a more complex molecule than the uniaxial. However, it is shown that once the model is obtained, it is general enough so that it can be used under different incidence angles, cell thickness and slight cell geometry variations. The model, which allows to obtain the static electromagnetic response of the PNLC cell for extreme excitations, has been validated by designing and manufacturing an electronically reconfigurable reflecting metasurface for phase control (reflectarray cell) with enough phase range to allow beam scanning. The novel designed cell provides millisecond-range relaxation times, improving substantially the response times of state-of-the-art
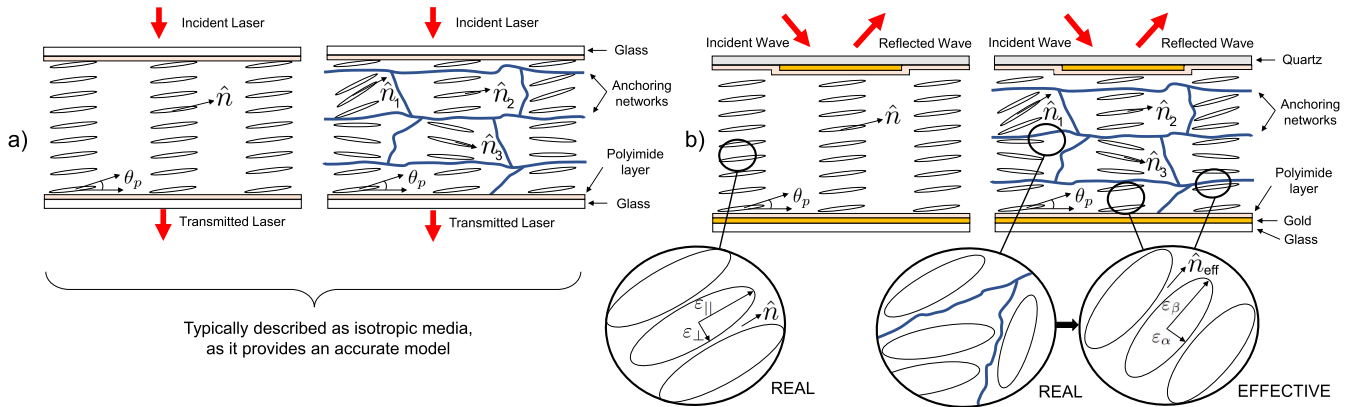
FIGURE 1. Sketch of a) transmissive and b) reflective LC cavities in repose state. Both conventional LC and PNLC cavities are shown on left and right, and the respective LC and PNLC molecular models are shown for the RF case.

LC-based reflectarray cells. The improvement is quantified at a cell level rather that an antenna level, given that studying the temporal evolution of the cell S-parameters facilitates the measurement and provides better accuracy than measuring the temporal evolution of the radiation pattern of a complete surface. Once the cell response is known, the radiation pattern of the whole device is analytic, and its temporal response matches that of the cell. As an additional contribution, the differences in the temporal improvement factor of the mixture in optics and RF, together with their cause, are analyzed.

This represents an interdisciplinary work, since it requires the convergence of two different technologies: the development of LC mixtures and the design and analysis of resonant metasurfaces at mm-wave, whose behaviour is completely different from optic devices.

II. THEORETICAL BACKGROUND

A. CONVENTIONAL LC

Given the anisotropic and inhomogeneous orientation of rod-like molecules of conventional LCs in a cavity, an uniaxial permittivity model is required to describe it. Eq. (1) relates the tilt angle of the conventional LC molecules with the macroscopic permittivity tensor.

$$\overline{\overline{\varepsilon_r}}(\overline{r}, t) = \varepsilon_\perp \overline{\overline{I}} + \Delta\varepsilon_r \hat{n}(\overline{r}, t) \otimes \hat{n}(\overline{r}, t), \qquad (1)$$

where $\overline{\overline{I}}$ is the 3×3 identity matrix, $\Delta\varepsilon_r = \varepsilon_\| - \varepsilon_\perp$ is the dielectric anisotropy, $\varepsilon_\|$ and $\varepsilon_\perp$ are the parallel and perpendicular dielectric constants, and $\hat{n}(\overline{r}, t)$ is the macroscopic vector that defines the local orientation of the LC molecules, which will vary along $\overline{r}$ when an electric field is applied. Since in RF the phase shift is created by the resonances, and $\overline{\overline{\varepsilon_r}}$ determines the resonances frequency shift upon external bias excitation, a larger dielectric anisotropy facilitates designing structures with larger phase range and bandwidth. The value of $\hat{n}(\overline{r}, t)$ for a conventional nematic LC with uniaxial molecules can be obtained by solving the Ericksen-Leslie equation [17], [30], which considers the elastic properties of the material and predicts the LC molecule rotation for a given excitation.

In cavities filled with conventional LCs (Fig. 1), a molecule switching plane and pretilt angle θ_p of the LC director is defined by placing and rubbing a thin polyimide layer on the enclosing plates. In thin cells, such as those used in optic devices, the polyimide provides an anchoring energy that aligns the molecules under no external excitation [31]. In thick cells, this effect is diluted, resulting in even larger relaxation times. However, the slow transition times of LC-based mm-wave reflecting surfaces are rarely analyzed, as will be seen. In most of the research works and even in some commercial LC devices (e.g. Kymeta [32]) a slow second-scale response is assumed [5], [12], which is insufficient for some applications. The modelling presented in this section, however, does not apply to PNLC mixtures.

B. POLYMER NETWORK LC (PNLC)

A PNLC consists of a conventional nematic LC doped with a reactive mesogen (RM), which is polymerized in situ inside the cavity. In our case, the RM is in itself a LC, which will align with the conventional LC. Upon polymerization the RM becomes an aligned polymer, which will act as an alignment agent in the volume of the LC. If the polymer is cured while the mixture is in a relaxed state, the polymer network will promote the relaxed alignment of the conventional LC in the whole volume of the cavity. Consequently higher bias fields must be applied to switch the cavity (in the order of 1-10 V/μm depending on the cavity thickness and the dopant content) and a much reduced relaxation time is achieved. In fact, the response time depends on the domain size (i.e. the monomer concentration) rather than on the cavity thickness, and therefore could be advantageous in larger cavity LC devices (i.e. lower frequencies) whose temporal response would be degraded using conventional LCs. A second side effect of the polymerization is that not only will the polymer itself not switch with the applied field, but also a significant part of the remaining conventional LC will be anchored so strongly to the rigid polymer network that it will not realign with any applied field of a reasonable magnitude. Therefore, while PNLCs accelerate how fast
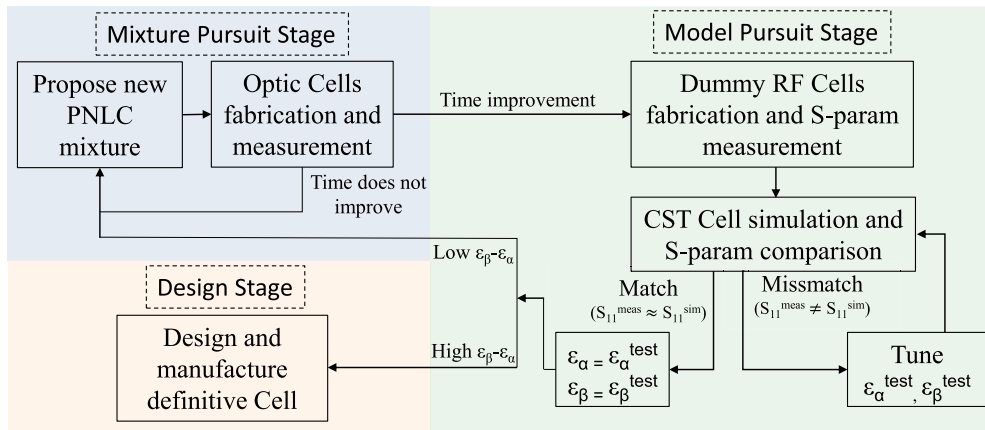
FIGURE 2. Process flow followed in this paper. First, in a mixture pursuit stage, the new PNLC mixture is proposed and its performance is first measured in optics. If the time response improvement is satisfactory, in the model pursuit stage the mixture is iteratively modelled from a mm-wave S-parameters measurement and by comparing it with CST simulations. Finally, if the mixture tunability is enough at mm-wave, the model can be used to design and manufacture a definitive cell.

$\hat{n}(\bar{r}, t)$ relaxes, it comes with a reduction in permittivity tuning range.

As mentioned above, when compared to pure LCs, whose elastic constants and other material properties allow for modelling both in statics and dynamics, PNLCs are harder to model given that the RM material (typically between 1% and 20%) is not switchable once polymerized. Therefore, computing $\hat{n}(\bar{r}, t)$ is not feasible. As a consequence, some works tried to approximate the PNLC dynamics by adding an auxiliary term to the Ericksen-Leslie equation using an effective electric field for the relaxation stage [33], valid only for small excitations and reorientation angles. Alternatively, its static behaviour could be modelled by using a range of effective scalar permittivities, $\varepsilon_{eff,max}$ and $\varepsilon_{eff,min}$ ($\Delta\varepsilon_{eff} = \varepsilon_{eff,max} - \varepsilon_{eff,min}$), which yields reasonable results in phase-shifting optic devices under the isotropic assumption. However, in the case of RF metasurfaces with resonators, and given the complexity of the electric fields induced by these, the anisotropy has considerable effects on the resulting phase [34] and the effective permittivity model must include it to properly generalize. Therefore, to design a structure requires obtaining $\hat{n}(\bar{r}, t)$ from measurement data, at least for some steady states. In this paper the dielectric permittivity (which intrinsically includes $\hat{n}(\bar{r}, t)$) will be modelled using an uniaxial effective anisotropic model deduced from measurements at the relaxed ($V = 0$) and maximum ($V = V_{sat}$) excitation states. Since both steady states are homogeneous for conventional LCs, the effective permittivity will be also assumed to be homogeneous for both in the PNLC model. It will be shown that, although the complete LC elastic model can not be used in PNLCs, the proposed model is capable of capturing the static behaviour of the mixture if effective values are considered, which enables designing different structures. The details of the model derivation are explained in Section III.

III. CHARACTERIZATION OF MM-WAVE PNLC CELLS
In this section, the PNLC is characterized from an electromagnetic point of view at mm-wave frequencies, obtaining effective permittivity values that can later be used in a design procedure using this specific mixture. The model will be derived from measurements of experimental cells in RF. To do so, a monomer (RMM34C provided by Merck [35]) 20 wt% will be mixed with a LC host that allows polymerization (not all LCs can be mixed) and that provides dielectric anisotropy at mm-wave bands (MDA-98-1602 by Merck). Likewise, the improvement in terms of cell dynamics will be evaluated by comparing the transition times of the PNLC mixture and the conventional LC, both in optics and RF. The complete process of obtaining a valid mixture, its modelling at mm-wave bands, and using it to design new structures is detailed in Fig. 2.

A. OPTICAL CELLS: MDA (CELL 1), MDA+PN (CELL 2)
To compare the improvement of response times in mm-wave and optics for the same mixtures, firstly both doped PNLC and undoped LC sample cells have been manufactured and measured in optical frequencies. This allows a quick check of the mixture capabilities to improve the temporal response of the LC molecules, and will allow a comparison between the optical and mm-wave cells. Given that the time reduction comes from a faster mechanical response of the LC molecules, an improvement measured in the optical regime will translate into an improvement in RF as well. However, as will be seen, the improvement will not be the same due to the different convergence of the magnitudes being measured (optical intensity and RF phase), and other fabrication matters. In PNLCs, relaxation times reduce as the monomer concentration increases. Here, a 20% concentration was chosen considering the trade-off between time response reduction versus tunability and the saturation bias voltage
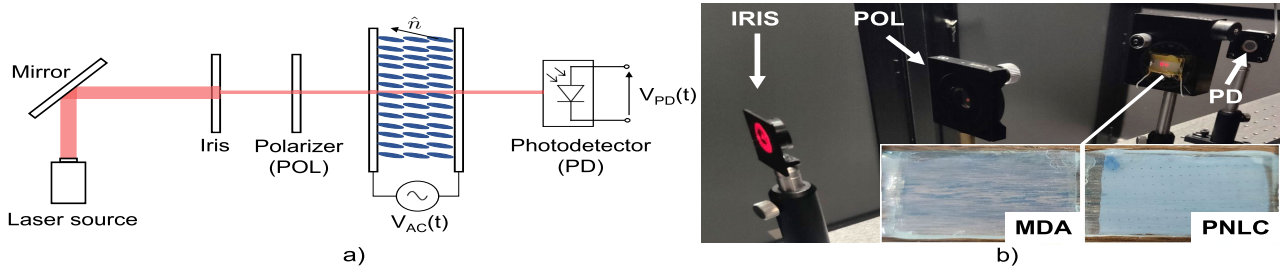
FIGURE 3. a) Schematic of the optical setup b) Picture of the setup. The inset shows the manufactured MDA and PNLC transmissive cells.
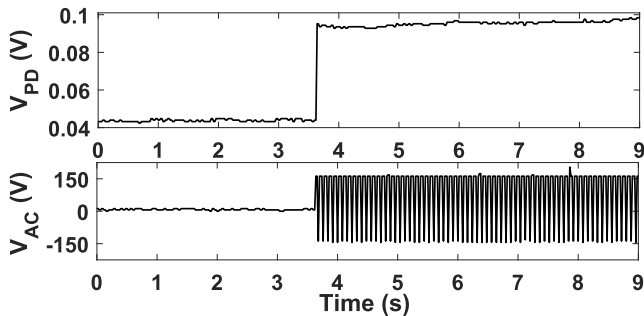

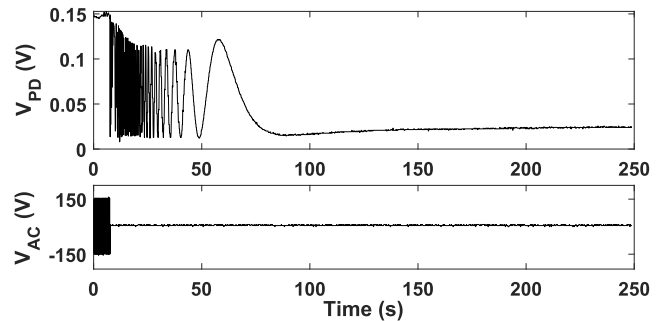**FIGURE 4.** Measured excitation transition of MDA transmissive cell 1.

FIGURE 5. Measured relaxation transition of MDA transmissive cell 1.

(V_{sat}) [36]. The transmissive sample cells consist in a $75\mu m$ thick LC cavity sandwiched between two glass plates with an inner indium tin oxide (ITO) conductive coating, transparent at optical frequencies with a 100nm rubbed polyimide. The cavity edges are sealed using UV-curing adhesive (NOA 81). This cell lacks resonators since in optical frequencies the simple transmission allows for the detection of the phase shift (several 360° cycles). In the doped case, the cells are filled with the mixture and subsequently UV-cured to create the anchoring networks. This can be seen in the cells of Fig. 3b, where the PNLC sample is visibly opaquer than the undoped sample. It is worth mentioning that the added manufacturing step of obtaining PNLC from conventional LC does not prevent the mass production of it, since it consists on a simple material mixing process.

After both the pure MDA and the PNLC cells are fabricated, their behavior is measured in the optical setup of Fig. 3. The cells are placed between a 632nm (474.7 THz) laser source and a photodetector, whose output $V_{PD}(t)$ is proportional to the incident radiant power and is captured using an oscilloscope.

To record the OFF-ON transition, a square 150V 1kHz excitation signal $V_{AC}(t)$ is applied to the cell, and for the ON-OFF transition the excitation is dropped to 0V. Fig. 4 and 5 respectively show the measured ON and OFF transitions of the undoped cell 1 (MDA). Both the LC biasing voltage $V_{AC}(t)$ and the photodetector output $V_{PD}(t)$ are shown. Fig. 6 shows the measured transition of the doped cell 2 (MDA+PN). As can be observed, the excitation transitions are equally fast in both cases (<20ms from 10% to
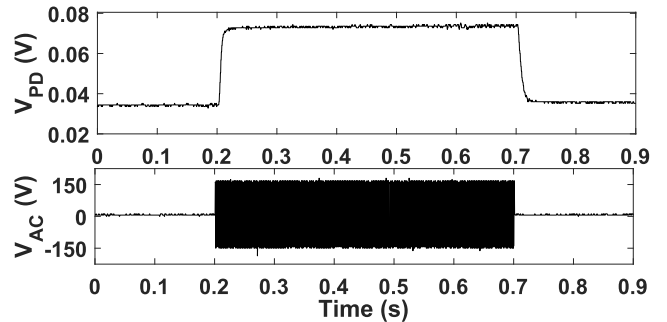

FIGURE 6. Measured temporal transitions of PNLC transmissive cell 2.

90%), but the relaxation times are greatly improved in the PNLC cells, as they took 11ms to relax as compared to 32s in the MDA case (90%-10% in number of 2π optical oscillations). Note that the 150V applied in this case, which is a large voltage, is necessary for characterization (LC director at 90°), but during a normal operation most of the molecules will be at intermediate states and therefore lower voltages are expected. Moreover, this voltage could be reduced by using a host LC that shows higher anisotropy and lower viscosity [2]. Additionally, depending on the application, a lower polymer concentration can be used, which reduces V_{sat}.

B. MM-WAVE CELLS: MDA (CELL 3), MDA+PN (CELL 4)
Exploiting that MDA is dielectrically anisotropic in mm-wave bands, a characterization is performed to study the dielectric tunability and losses. Consequently, undoped (Cell 3) and doped (Cell 4) mm-wave sample cells are

manufactured and measured to characterize the electromagnetic properties of the materials and to measure its temporal response. In this case, the mm-wave cells with resonators are reflective since it facilitates the measurement with a vector network analyzer (VNA).

1) MODEL DERIVATION

From Eq. (1), the permittivity matrices in both extreme states are:

$$\bar{\bar{\varepsilon}}_{r,OFF} = \begin{pmatrix} \varepsilon_\alpha & 0 & 0 \\ 0 & \varepsilon_\beta & 0 \\ 0 & 0 & \varepsilon_\alpha \end{pmatrix} ; \ \bar{\bar{\varepsilon}}_{r,ON} = \begin{pmatrix} \varepsilon_\alpha & 0 & 0 \\ 0 & \varepsilon_\alpha & 0 \\ 0 & 0 & \varepsilon_\beta \end{pmatrix} \tag{2}$$

In Cell 3, which contains conventional LC, the parameter extraction process provides the conventional values of $\varepsilon_\beta = \varepsilon_{||}$ and $\varepsilon_\alpha = \varepsilon_\perp$. In PNLCs (Cell 4) these will be effective values, given that they actually do not adapt uniaxial structure (see Fig. 1), as aforementioned. The model consists on deriving these values from the S-parameter measurements of the cells. To do so, an iterative simulation process is followed to match the simulated response, with test $\varepsilon_\alpha, \varepsilon_\beta$ values, to the measurements in the entire band.

It is also important to note that these effective $\varepsilon_\alpha, \varepsilon_\beta$ differ from effective scalar permittivities $\varepsilon_{eff,max}, \varepsilon_{eff,min}$ of the isotropic model used for PNLC in optical devices. Note also that given that for Cell 3 (undoped) both $\varepsilon_{||}$ and $\varepsilon_\perp$ are known for the conventional MDA, together with its elastic constants and viscosity, the phase-voltages curves and the dynamics can be computed solving the Ericksen-Leslie equation and Eq. (1). However, the effective ε_α and ε_β of Cell 4 (doped) do not provide the same capability for PNLCs, as the elastic constants and viscosity of the new mixture can not be properly defined. Thus, the effective permittivity matrices obtained through the PNLC model are specific for the static extreme states, and therefore, a complete phase-voltage and dynamic characterization of the PNLC would require a measurement for each bias of interest. However, the model is general enough to enable accurate designs of any similar planar structure, cavity thickness and incidence angle suitable for phase manipulation of mm-waves, as will be seen in the following section.

The manufacturing details of Cells 3 and 4 are as follows. In this mm-wave case, gold resonators are grown on the inside of the superstrate using photolithography, which divides the structure in periodical unit cells, as showed in Fig. 7. The manufactured devices consist of a $75 \mu m$ thick LC cavity sandwiched between a top 1.25 mm thick quartz superstrate and a bottom ground plane made of $1 \mu m$ thick gold. Both the top and bottom substrates are treated with polyimide alignment layers like in the transmissive cells. The resonators increase the achievable phase range of the surface by adding resonances to the reflecting coefficient [5], [37]. Since the presence of a uniform ITO layer in the superstrate of reflective cells would incur losses, the gold resonators will also be
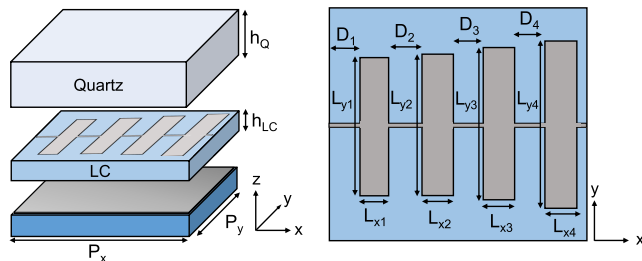

FIGURE 7. Unit cell structure of the reflective manufactured surfaces.

TABLE 1. Dimensions (mm) of the manufactured sample reflective cells 3&4 and PNLC reflectarray cell 5.

Param.	Cells 3&4	Cell 5	Param.	Cells 3&4	Cell 5
P_x	1.96	1.4	L_{x3}	0.19	0.19
P_y	1.42	1.4	L_{x4}	0.18	0.17
D_1	0.1857	0.125	L_{y1}	0.6322	0.68
D_2	0.3884	0.195	L_{y2}	0.6765	0.75
D_3	0.1448	0.12	L_{y3}	0.738	0.81
D_4	0.2586	0.125	L_{y4}	0.7995	0.86
L_{x1}	0.133	0.17	h_{LC}	0.075	0.045
L_{x2}	0.18	0.18	h_Q	1.25	0.43

used as electrodes to bias the LC instead of using ITO. From this structure, two identical dummy cells are manufactured, one containing MDA (Cell 3) and another containing the MDA+PN mixture (Cell 4). The sample dimensions of these cells can be found in Table 1. Fig. 8 shows a picture of the manufactured Cell 3.

The S_{11} parameter of both manufactured cells has been measured in periodical environment with the same $V_{AC}(t)$ by means of a quasi-optical free space measurement setup and a VNA connected to a pair of horn antennas. To obtain a macroscopic S_{11} measurement of the unit cell, all the unit cells are short-circuited and connected to $V_{AC}(t)$. The S_{11} has been used to derive the values of the permittivity matrix using an iterative process that compares the measured and modelled S_{11} parameters, as shown in Fig. 2. That is, in order to obtain the effective dielectric permittivity components for any given bias, as well as the losses of both the MDA and PNLC materials, a fitting procedure from a full-wave electromagnetic simulation (CST Studio [38]) to the measured reflection coefficient is performed along the entire frequency band. In the simulation, the complex dielectric permittivity components of the uniaxial model are carefully adjusted in each iteration. The classical infinite array (unit cell and local periodicity) approach is used to analyze the structure, thus considering the coupling and all the neighbouring effects of the cells [39]. As previously mentioned, layer homogeneity is considered by averaging the local director angle across z, which significantly reduces the computational cost and has relatively low effects in accuracy [40]. This is particularly precise in the extreme biasing states of conventional LCs, where the angle of the director is either 0° or 90° across almost the entire cell.
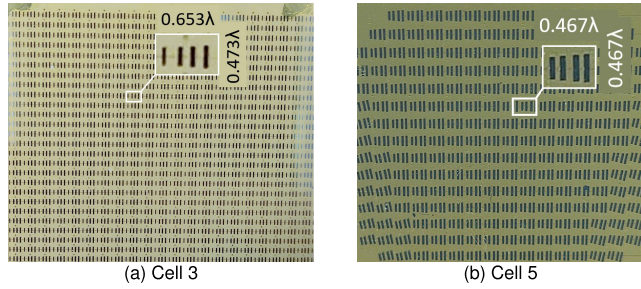
FIGURE 8. Photo of the manufactured reflective Cell 3 (a) and final PNLC-based reflectarray Cell 5 (b).
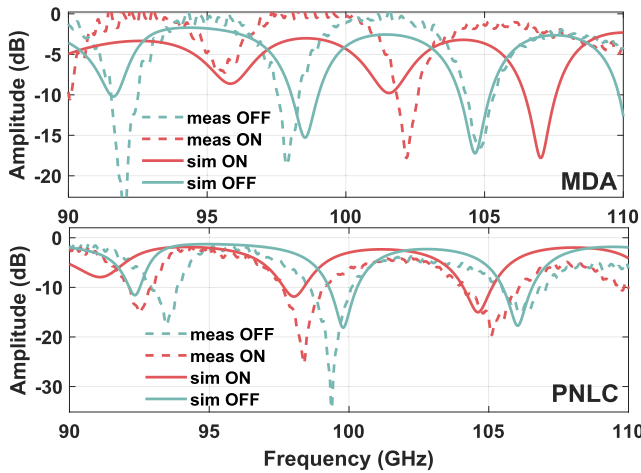

FIGURE 9. Measured S_{11} amplitude of MDA (top) and PNLC (bottom) cells 3 and 4 as a function of frequency for a permittivity matrix characterization, from which the data of Table 2 is obtained. The reconstructed (simulated) S_{11} amplitude according to this extracted data (iterative process solution) is also shown. Extreme states in permanent regime are shown, with 150V (ON) and 0V (OFF) V_{AC} amplitudes, for a 45° incidence angle.

2) CHARACTERIZATION RESULTS AND TEMPORAL EVALUATION

The characterization results of both MDA (Cell 3) and MDA+PN (Cell 4) mixtures, obtained after the model derivation of the previous subsection, are shown in Table 2. To show that the obtained results are correct, Fig. 9 shows the measured and the simulated amplitude of the reflection coefficient (S_{11}) for both cells after sufficient time has passed (stationary regime), for null and high amplitudes of V_{AC} (OFF and ON states), and at an incidence angle of 45°. The simulation results have been obtained using the matrices of Eq. (2), considering the derived parameters reported in Table 2. As can be seen, the simulation matches the measurements of Cells 3 and 4. For the PNLCs, a 3X reduction in the dielectric tunability ($\Delta\varepsilon = \varepsilon_{||} - \varepsilon_\perp = 0.59$ in MDA and $\Delta\varepsilon = 0.19$ in PNLC) and increased cell losses (around -3dB in measurement data) as expected is observed.

The temporal transitions of both MDA and PNLC structures are also recorded in the quasi-optical bench, by externally triggering VNA captures in sync with the LC driving transitions. The measurement is performed at 97GHz, where
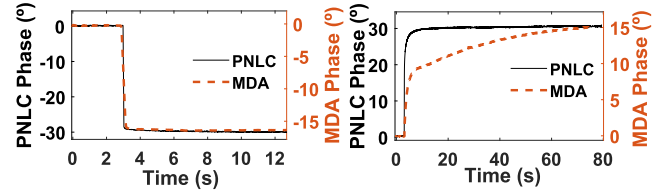

FIGURE 10. Measured MDA and PNLC excitation (left) and relaxation (right) S_{11} phase transitions in reflective cell samples at 97GHz.
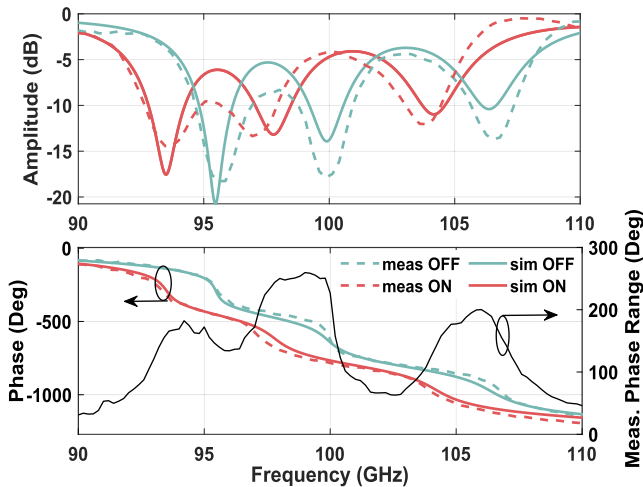
TABLE 2. LC parameters and Characterization results at 100 GHz.

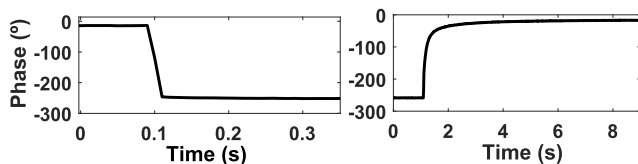| Param.	GT3-23001	GT3+PN	MDA-98-1602	MDA+PN
$\varepsilon_{||}$	3.27	N/A	3.28	2.69^*
$\varepsilon_\perp$	2.47	N/A	2.7	2.5^{**}
$tan\delta_{||}$	0.015	N/A	0.015	0.02^*
$tan\delta_\perp$	0.02	N/A	0.02	0.021^{**}
V_{sat}^{***}	15V	N/A	$\sim 15V$	$\sim 150V$

* Effective ε_β ** Effective ε_α ***In $75\mu m$-thick cells

the phase range is maximum, and at an incidence angle of 45°. In this case, the S_{11} phase is measured, instead of amplitude, since it is a more appropriate magnitude to measure temporal responses. As shown in Fig. 10, the excitation transition is relatively quick in both MDA and PNLC cases (<40ms), while the 90%-10% relaxation time is reduced by a factor 50X in the PNLC sample, from 42s to 800ms. The phase ranges are not directly comparable since the device was not optimized for the permittivities of the MDA nor the PNLC. Consequently, very small phase shifts are seen and each device has a completely different resonant behaviour. However, it can be appreciated how the PNLC is much faster in the relaxation transition while their behaviour is identical in the excitation stage. The improvement in response time is, as expected, significant when the LC is doped with polymer.

Table 3 shows the performance of all the manufactured and tested cells in terms of decay times. It can be noted that the Cells 1 and 3, which contain conventional MDA and are designed for optics and RF respectively, exhibit different decay times although both have the same thickness. This can be attributed to different sources: (1) The manufacturing tolerances of $\pm 2\mu m$ for the LC thickness, which only relates to a time variation of a 5%. (2) The different magnitude being measured, i.e. optical intensity and S_{11} phase, whose convergence can not be directly compared even if the LC molecular structure is the same. In other words, the 90% convergence of one magnitude can be achieved earlier than the other for the same LC state. Although this effect can be extended to PNLCs, the discrepancy in response time for the polymer doped LCs in the optical and RF configurations (Cells 2 and 4), as seen in Table 3, can be almost entirely assigned assigned to (3) the different irradiation conditions in the UV curation process. Since the top electrode of the resonant RF cells contains metallic dipoles, the volume underneath them was not completely polymerized, as opposed to the transmissive optical cells whose mixture is completely

FIGURE 11. Reflection coefficient amplitude (top) and phase (bottom) of the PNLC-based reflectarray cell 5.

FIGURE 12. Measured excitation (left) and relaxation (right) S_{11} phase transitions of the designed PNLC cell at 99GHz.

TABLE 3. Measured temporal performance of LC and PNLC cells.

Sample	Material	Thickness	Relax. Time	Improv.
Optical Cell 1	MDA	$75\mu m$	32s	~3000X
Optical Cell 2	MDA+PN	$75\mu m$	11ms	
RF Cell 3	MDA	$75\mu m$	42s	~50X
RF Cell 4	MDA+PN	$75\mu m$	800ms	
RF Cell 5	MDA+PN	$45\mu m$	210ms*	

* Measured 90%-10% to the target 180° phase shift

The amplitude and phase of the reflection coefficient of the manufactured reflectarray, shown in Fig. 11, has been measured at an incidence angle of 30°. This angle was deliberately changed from the one used during the parameter derivation (45°) to validate the generality of the permittivity model. As can be seen, the effective uniaxial model allows the prediction of the cell behavior even in a different structure and incident angle, showing geometry-independence. Given the limited dielectric tuning of the PNLC, the phase range is reduced but still sufficient to achieve the desired 180° in three different bands (around 94 GHz, 98.5 GHz and 106 GHz), being the 97.1 GHz-100.3 GHz the most prominent one as shown in Fig. 11. This phase range allows for a 1-bit quantization reflectarray design. In terms of antenna performance, this compromises the gain and sidelobe level when compared to a 360° cell [46] but still continuous scanning. Fig. 12 shows the temporal response of the reflectarray, measured at the frequency of greatest phase range following the same procedure as in Section III-B2. The 180° 10%-90% ON transition takes 12ms while the 90%-10% OFF transition takes 210ms, representing the fastest achieved relaxation transition in a thick mm-wave LC-based reflectarray with enough phase range, to the best of the authors knowledge. Table 4 compares this work to previous LC reflectarray works. To facilitate a fair comparison in terms of electromagnetic performance and temporal response, the simulated results of the Cell 5 containing pure MDA have also been included, given the accuracy presented by its model.

To obtain a cell exhibiting larger phase range with such a reduced dielectric tunability, imposed by the PNLC, would require a reduction of the cavity thickness of the structure leading to loss increase and poor coupling [47]. A potential alternative is doping new LC materials whose dielectric anisotropy $\Delta\varepsilon$ is large at mm-wave frequencies, so that when mixed with the polymer the effective tunable anisotropy $\Delta\varepsilon_{eff}$ results sufficient to achieve 360°. One potential candidate is the LC GT7-29001, that in preliminary experiments shows to be compatible with polymerization. The reduction in temporal response could be further improved increasing the polymer network concentration within the mixture, at the expense of lower effective dielectric tuning range and an increase of the required driving voltage. Moreover, the use of new LC generations capable of polymerizing, showing greater dielectric anisotropy in mm-wave bands, and with a reduced saturation voltage, could pave the way to tenths of millisecond relaxation times while using bias excitations of

polymerized throughout the whole volume. This makes some LC molecules of the PNLC RF cells to rotate slower than those of the cells that do not include metallic resonators. Nevertheless, the relaxation time was still very much improved with respect to the conventional LC case. Therefore, the 50X factor might be enhanced by intensifying the irradiation conditions, or by a careful design of the resonators in such a way that they cover a small superstrate area while still fulfilling their RF purpose.

Table 2 includes the results of two additional cells, manufactured to evaluate the performance of the polymer network mixed with another LC typically used in microwaves (GT3-23001 by Merck). However, the dopant was not polymerizable in the presence of GT3, which is is likely to be caused by radical scavengers in the GT3 mixture, or due to UV-induced decomposition of one or several components of GT3, inhibiting the polymerization.

IV. PNLC-BASED REFLECTARRAY DESIGN

In order to validate the model and characterization of the dielectric permittivity of section III, a reflective PNLC cell (Cell 5) was designed, manufactured and tested using the data of Table 2. In this case, the cell (reflectarray cell) is designed targeting a fast device exhibiting a phase range of at least 180°, to show its applicability. This cell was manufactured and tested using the same process as in Section III-B2. Fig. 8b shows a picture of the manufactured surface, whose dimensions can be found in Table 1.

TABLE 4. Comparison of different LC reflectarray cell works.

Work	[5]	[7]	[41]	[42]	[43]	[44]	[17]		This Work
Technology	LC	LC	LC	LC	LC	LC	LC+OD	LC+OD	PNLC
LC material	GT3-23001	GT3-23001	BL006	BL006	HFUT-HB01	HFUT-HB01	GT3-23001	MDA	MDA+PN
Freq. (GHz)	100	78	10	35	100	120	100	100	100
Losses (avg)	6dB	12dB	15dB	7dB	12dB	6dB	6dB	7dB	9dB
Phase Range	360°	270°	200°	250°	350°	300°	360°	270°	180°
Meas. Ton	NA	NA	NA	NA	NA	NA²	50ms	NA	12ms
Meas. Toff	NA	NA	NA	NA	NA	NA²	5s	NA	210ms
Est. Ton[1]	4s	2s	3s	1s	NA	NA²	NA	10ms	NA
Est. Toff[1]	40s	18s	200s	14s	NA	NA²	NA	15s	NA
Thickness	$75\mu m$	$50\mu m$	$500\mu m$	$127\mu m$	$60\mu m$	$45\mu m$	$75\mu m$	$45\mu m$	$45\mu m$

[1] Estimated considering a 90%-10% RF phase change from the exponential time constant expressions found in [45]. OD indicates overdrive [17].
[2] Declared 200ms optical response.

few volts at the same thickness ranges. In regards to the circuitry required to scan the beam, the physical manufactured structure is identical to the one implemented here. However, the external driving circuitry to implement the three classical strategies that allow biasing each unit cell independently (direct, passive and active addressing), reported in the state of the art [30], will require the handling of high-voltages due to the PNLC.

V. CONCLUSION

A fast PNLC mixture for mm-wave phase-shift metasurfaces has been presented and evaluated. The mixture has been modelled based on the two extreme biasing states by using an uniaxial effective permittivity model, obtained experimentally, facilitating the design of fast LC-based structures. The model is accurate and general enough to exhibit robustness to varying angle of incidence and cell dimensions, contrary to the isotropic effective model commonly used in optical phase-shift PNLC cells. Compared to a conventional LC, the dielectric tunability is reduced by more than a factor of two while the saturation voltage increases. The mixture presented in this work (MDA+PN), relaxed 50 times faster than the pure MDA in RF cells. Given the reduced irradiation conditions during the PNLC curation process in RF cells due to the metallic resonators, this improvement factor is smaller than in optical cells. A relaxation time of 210ms is achieved in a $45\mu m$-thick cell that operates at W-band when 150V biasing voltage is employed, although better results can be expected under thinner cells, i.e. higher frequency metasurfaces. Alternatively, improved PNLC curation conditions could further reduce these results, which requires the development of novel manufacturing strategies with respect to the traditional PNLC methods.

REFERENCES

[1] D. F. Sievenpiper, J. H. Schaffner, H. J. Song, R. Y. Loo, and G. Tangonan, "Two-dimensional beam steering using an electrically tunable impedance surface," *IEEE Trans. Antennas Propag.*, vol. 51, no. 10, pp. 2713–2722, Oct. 2003.

[2] E. Basar, M. D. Renzo, J. D. Rosny, M. Debbah, M. Alouini, and R. Zhang, "Wireless communications through reconfigurable intelligent surfaces," *IEEE Access*, vol. 7, pp. 116753–116773, 2019.

[3] M. A. El Mossallamy, H. Zhang, L. Song, K. G. Seddik, Z. Han, and G. Y. Li, "Reconfigurable intelligent surfaces for wireless communications: Principles, challenges, and opportunities," *IEEE Trans. Cogn. Commun. Netw.*, vol. 6, no. 3, pp. 990–1002, Sep. 2020.

[4] Y.-C. Liang, J. Chen, R. Long, Z.-Q. He, X. Lin, C. Huang, S. Liu, X. S. Shen, and M. D. Renzo, "Reconfigurable intelligent surfaces for smart wireless environments: Channel estimation, system design and applications in 6G networks," *Sci. China Inf. Sci.*, vol. 64, no. 10, pp. 1–21, Oct. 2021.

[5] G. Perez-Palomino, M. Barba, A. J. Encinar, R. Cahill, R. Dickie, P. Baine, and M. Bain, "Design and demonstration of an electronically scanned reflectarray antenna at 100 GHz using multiresonant cells based on liquid crystals," *IEEE Trans. Antennas Propag.*, vol. 63, no. 8, pp. 3722–3727, Aug. 2015.

[6] J.-F. Lv, C. Ding, Z. Zhu, X. Li, F.-Y. Meng, J.-Q. Han, T. Jin, and Q. Wu, "Tunable liquid crystal frequency selective surface with the compact unit cell, large tuning range, and the passband of flat-top and sharp roll-off," *J. Phys. D, Appl. Phys.*, vol. 54, no. 31, Aug. 2021, Art. no. 315001.

[7] S. Bildik, S. Dieter, C. Fritzsch, W. Menzel, and R. Jakoby, "Reconfigurable folded reflectarray antenna based upon liquid crystal technology," *IEEE Trans. Antennas Propag.*, vol. 63, no. 1, pp. 122–132, Jan. 2015.

[8] S. V. Hum and J. Perruisseau-Carrier, "Reconfigurable reflectarrays and array lenses for dynamic antenna beam control: A review," *IEEE Trans. Antennas Propag.*, vol. 62, no. 1, pp. 183–198, Jan. 2014.

[9] E. Carrasco, M. Barba, and J. A. Encinar, "X-band reflectarray antenna with switching-beam using PIN diodes and gathered elements," *IEEE Trans. Antennas Propag.*, vol. 60, no. 12, pp. 5700–5708, Dec. 2012.

[10] T. Debogovic and J. Perruisseau-Carrier, "Low loss MEMS-reconfigurable 1-bit reflectarray cell with dual-linear polarization," *IEEE Trans. Antennas Propag.*, vol. 62, no. 10, pp. 5055–5060, Oct. 2014.

[11] A. Singh, M. Andrello, E. Einarsson, N. Thawdarl, and J. M. Jornet, "A hybrid intelligent reflecting surface with graphene-based control elements for THz communications," in *Proc. IEEE 21st Int. Workshop Signal Process. Adv. Wireless Commun. (SPAWC)*, May 2020, pp. 1–5.

[12] R. Jakoby, A. Gaebler, and C. Weickhmann, "Microwave liquid crystal enabling technology for electronically steerable antennas in SATCOM and 5G millimeter-wave systems," *Crystals*, vol. 10, no. 6, p. 514, Jun. 2020.

[13] J. Wu, Z. Shen, S. Ge, B. Chen, Z. Shen, T. Wang, C. Zhang, W. Hu, K. Fan, W. Padilla, Y. Lu, B. Jin, J. Chen, and P. Wu, "Liquid crystal programmable metasurface for terahertz beam steering," *Appl. Phys. Lett.*, vol. 116, no. 13, Mar. 2020, Art. no. 131104.

[14] T.-J. Chen, G.-J. Lin, B.-Y. Chen, J.-J. Wu, and Y.-J. Yang, "Fast-response liquid crystal display by the VA-IPS display mode with nematic liquid crystal and polymer networks," *Proc. SPIE*, vol. 8475, Oct. 2012, Art. no. 847513.

[15] R. Camley, Z. Celinski, Y. Garbovskiy, and A. Glushchenko, "Liquid crystals for signal processing applications in the microwave and millimeter wave frequency ranges," *Liquid Cryst. Rev.*, vol. 6, no. 1, pp. 17–52, Jan. 2018.

[16] G. Thalhammer, W. R. Bowman, D. G. Love, J. M. Padgett, and M. Ritsch-Marte, "Speeding up liquid crystal SLMs using overdrive with phase change reduction," *Opt. Exp.*, vol. 21, no. 2, pp. 1779–1797, Jan. 2013.

[17] R. Guirado, G. Perez-Palomino, M. Ferreras, E. Carrasco, and M. Cano-Garcia, "Dynamic modelling of liquid crystal-based metasurfaces and its application to reducing reconfigurability times," *IEEE Trans. Antennas Propag.*, early access, Oct. 3, 2022, doi: 10.1109/TAP.2022.3209734.

[18] A. Jiménez-Sáez, A. Asadi, R. Neuder, D. Wang, and R. Jakoby, "Liquid crystals: The way to scalable and practical reconfigurable intelligent surfaces in 6G," TechRxiv, to be published.

[19] O. Melnyk, Y. Garbovskiy, D. Bueno-Baques, and A. Glushchenko, "Electro-optical switching of dual-frequency nematic liquid crystals: Regimes of thin and thick cells," *Crystals*, vol. 9, no. 6, p. 314, Jun. 2019.

[20] J. Sun, S.-T. Wu, and Y. Haseba, "A low voltage submillisecond-response polymer network liquid crystal spatial light modulator," *Appl. Phys. Lett.*, vol. 104, no. 2, Jan. 2014, Art. no. 023305.

[21] J. Sun and S.-T. Wu, "Recent advances in polymer network liquid crystal spatial light modulators," *J. Polym. Sci. B, Polym. Phys.*, vol. 52, no. 3, pp. 183–192, Feb. 2013.

[22] Y.-H. Fan, Y.-H. Lin, H. Ren, S. Gauza, and S.-T. Wu, "Fast-response and scattering-free polymer network liquid crystals for infrared light modulators," *Appl. Phys. Lett.*, vol. 84, no. 8, pp. 1233–1235, Feb. 2004.

[23] D. G. Love, K. A. Kirby, and A. R. Ramsey, "Sub-millisecond, high stroke phase modulation using polymer network liquid crystals," *Opt. Exp.*, vol. 18, no. 7, pp. 7384–7389, Mar. 2010.

[24] J. L. West, G. Zhang, A. Glushchenko, and Y. Reznikov, "Fast birefringent mode stressed liquid crystal," *Appl. Phys. Lett.*, vol. 86, no. 3, Jan. 2005, Art. no. 031111.

[25] Z. Yin, C. Wan, G. Deng, A. Zheng, P. Wang, Y. Yang, S. Gao, J. Yang, F. Cai, Z. Li, and H. Lu, "Fast-tunable terahertz metamaterial absorber based on polymer network liquid crystal," *Appl. Sci.*, vol. 8, no. 12, p. 2454, Dec. 2018.

[26] F. Peng, H. Chen, S. Tripathi, J. R. Twieg, and S.-T. Wu, "Fast-response infrared phase modulator based on polymer network liquid crystal," *Opt. Mater. Exp.*, vol. 5, no. 2, pp. 265–273, Feb. 2015.

[27] H. Fujikake, T. Kuki, T. Nomoto, Y. Tsuchiya, and Y. Utsumi, "Thick polymer-stabilized liquid crystal films for microwave phase control," *J. Appl. Phys.*, vol. 89, no. 10, pp. 5295–5298, May 2001.

[28] T. Nguyen, S. Umeno, H. Higuchi, H. Kikuchi, and H. Moritake, "Improvement of decay time in nematic-liquid-crystal-loaded coplanar-waveguide-type microwave phase shifter by polymer stabilizing method," *Jpn. J. Appl. Phys.*, vol. 53, no. 1S, Jan. 2014, Art. no. 01AE08.

[29] R. James, F. A. Fernandez, S. E. Day, S. Bulja, and D. Mirshekar-Syahkal, "Accurate modeling for wideband characterization of nematic liquid crystals for microwave applications," *IEEE Trans. Microw. Theory Techn.*, vol. 57, no. 12, pp. 3293–3297, Dec. 2009.

[30] D.-K. Yang and S.-T. Wu, "Fundamentals of liquid crystal devices," in *Wiley Series in Display Technology*, 2nd ed. Hoboken, NJ, USA: Wiley, 2014, pp. 1–570.

[31] L. Weng, P.-C. Liao, C.-C. Lin, T.-L. Ting, W.-H. Hsu, J.-J. Su, and L.-C. Chien, "Anchoring energy enhancement and pretilt angle control of liquid crystal alignment on polymerized surfaces," *AIP Adv.*, vol. 5, no. 9, Sep. 2015, Art. no. 097218.

[32] A. Bautista, R. Stevenson, M. Sazegar, T. Schlichter, and T. Heyn, "Dynamically reconfigurable metasurface antennas for mobile connectivity in 5G non-terrestrial networks," in *IEEE MTT-S Int. Microw. Symp. Dig.*, Jun. 2022, pp. 994–997.

[33] D.-K. Yang, Y. Cui, H. Nemati, X. Zhou, and A. Moheghi, "Modeling aligning effect of polymer network in polymer stabilized nematic liquid crystals," *J. Appl. Phys.*, vol. 114, no. 24, 2013, Art. no. 243515.

[34] G. Perez-Palomino, P. Baine, R. Dickie, M. Bain, A. José Encinar, R. Cahill, M. Barba, and G. Toso, "Design and experimental validation of liquid crystal-based reconfigurable reflectarray elements with improved bandwidth in F-band," *IEEE Trans. Antennas Propag.*, vol. 61, no. 4, pp. 1704–1713, Apr. 2013.

[35] *Merck KGaA*. Accessed: Apr. 18, 2022. [Online]. Available: www.merckgroup.com

[36] C. C. Vela, "Diseño y fabricación de dispositivos basados en cristal líquido polimérico," Ph.D. thesis, Señales, Sistemas y Radiocomunicaciones, Universidad Politécnica de Madrid, Madrid, Spain, 2012, p. 198.

[37] R. Faqiri, C. Saigre-Tardif, G. C. Alexandropoulos, N. Shlezinger, M. F. Imani, and P. del Hougne, "PhysFad: Physics-based end-to-end channel modeling of RIS-parametrized environments with adjustable fading," *IEEE Trans. Wireless Commun.*, early access, Aug. 15, 2022, doi: 10.1109/TWC.2022.3196834.

[38] *CST Studio*. Accessed: Feb. 4, 2022. [Online]. Available: www.cst.com

[39] J. Huang and J. A. Encinar, *Reflectarray Antennas*. Hoboken, NJ, USA: Wiley, 2007.

[40] G. Perez-Palomino, R. Florencio, A. José Encinar, M. Barba, R. Dickie, R. Cahill, P. Baine, M. Bain, and R. Rafael Boix, "Accurate and efficient modeling to calculate the voltage dependence of liquid crystal-based reflectarray cells," *IEEE Trans. Antennas Propag.*, vol. 62, no. 5, pp. 2659–2668, May 2014.

[41] W. Hu, M. Y. Ismail, R. Cahill, J. A. Encinar, V. F. Fusco, H. S. Gamble, D. Linton, R. Dickie, N. Grant, and S. P. Rea, "Liquid-crystal-based reflectarray antenna with electronically switchable monopulse patterns," *Electron. Lett.*, vol. 43, no. 14, p. 744, 2007.

[42] A. Moessinger, R. Marin, S. Mueller, J. Freese, and R. Jakoby, "Electronically reconfigurable reflectarrays with nematic liquid crystals," *Electron. Lett.*, vol. 42, no. 16, pp. 899–900, Aug. 2006.

[43] S.-Y. Sun, X. Yu, P.-J. Wang, C.-F. Wan, J. Yang, Z. Yin, G. Deng, and H.-B. Lu, "Electronically tunable liquid-crystal-based F-band phase shifter," *IEEE Access*, vol. 8, pp. 151065–151071, 2020.

[44] S. Gao, J. Yang, P. Wang, A. Zheng, H. Lu, G. Deng, W. Lai, and Z. Yin, "Tunable liquid crystal based phase shifter with a slot unit cell for reconfigurable reflectarrays in F-band," *Appl. Sci.*, vol. 8, no. 12, p. 2528, Dec. 2018.

[45] H. Wang, T. X. Wu, X. Zhu, and S.-T. Wu, "Correlations between liquid crystal director reorientation and optical response time of a homeotropic cell," *J. Appl. Phys.*, vol. 95, no. 10, pp. 5502–5508, May 2004.

[46] H. Yang, F. Yang, S. Xu, M. Li, X. Cao, J. Gao, and Y. Zheng, "A study of phase quantization effects for reconfigurable reflectarray antennas," *IEEE Antennas Wireless Propag. Lett.*, vol. 16, pp. 302–305, 2016.

[47] K. K. Karnati, Y. Yusuf, S. Ebadi, and X. Gong, "Theoretical analysis on reflection properties of reflectarray unit cells using quality factors," *IEEE Trans. Antennas Propag.*, vol. 61, no. 1, pp. 201–210, Jan. 2013.

ROBERT GUIRADO was born in Badalona, Spain. He received the B.Sc. and M.Sc. degrees in telecommunication systems engineering from Universitat Politècnica de Catalunya, Barcelona, Spain, in 2019 and 2021, respectively. He is currently pursuing the Ph.D. degree in reconfigurable intelligent surfaces based on liquid crystals with the Applied Electromagnetism Group (GEA), Universidad Politécnica de Madrid (UPM), Madrid, Spain.

GERARDO PEREZ-PALOMINO was born in Granada, Spain. He received the M.Sc. and Ph.D. degrees in telecommunication engineering from the Universidad Politécnica de Madrid (UPM), Madrid, Spain, in 2009 and 2015, respectively. Since 2008, he has been a Researcher with the Applied Electromagnetism Group (GEA), UPM. In 2019, he joined the Department of Signals, Systems, and Radio Communications, where he is currently an Associate Professor. He is involved in the development of reconfigurable antennas in millimeter and submillimeter wavelengths using liquid crystals and the design of devices based on planar periodic structures, including reflectarrays and transmitarrays. His research interests include analysis, characterization, modeling, and the design of antennas and microwave systems, and the electromagnetic and circuit theory.

MANUEL CAÑO-GARCÍA received the M.Sc. degree in physics and the M.Sc. degree in electronic engineering from the University of Granada, in 2013, the M.Sc. degree in nanotechnology from the Autonomous University of Madrid, in 2014, and the international Ph.D. degree (summa cum laude) in photonics from the Technical University of Madrid (UPM), in 2018 within a Spanish Official Grant (FPI 2014). He has been involved three European projects and four Spanish national projects. He did a two-year postdoctoral stay at the International Iberian Nanotechnology Laboratory, Braga, Portugal, with a Marie Skłodowska-Curie Actions Scholarship and currently a Distinguished Researcher with the CEMDATIC Center (UPM) with a Beatriz Galindo grant. His research interest includes the development of active photonics integrated circuits (PICs) with metamaterials or photonics crystals technologies for bio-sensing.

MORTEN A. GEDAY did his studies in Chemistry and Biotechnology, Aarhus University (DK), with an 8 Month stay in the chemistry department of chemistry in University of Calabria (IT). He did his Ph.D. in condensed matter physics in 2001, Oxford University (UK), with three months stay at Washington University (US) chemistry department in 2000. Having worked three years in a spin-off company in the UK, he was granted in 2004 an incorporation grant and 2005 a five-year Ramón y Cajal research fellowship at the UPM, which in 2008 was converted into an I3-fellowship which was again converted into a permanent position as Associate professor (Professor Titular) in 2012.

Since his incorporation at the UPM, his research has been centred on the development, characterisation, and simulation of liquid crystal devices, with applications outside conventional liquid crystal displays. He has co-authored more than 150 research articles and conference communications and has filed 7 patents. He has been the coordinator of three European project and IP of both private and public (regional and national) projects and participated in more than 15. He is the co-founder of the spin-off Alise Devices S.L. whose activities are based on three of the previously mentioned patents.

EDUARDO CARRASCO (Senior Member, IEEE) received the bachelor's degree in telecommunication engineering from the National Autonomous University of Mexico (UNAM), Mexico City, in 2000, and the Ph.D. degree in telecommunication engineering from the Technical University of Madrid (UPM), Madrid, Spain, in 2008. From January to April 2008, he visited the Microwave Engineering Laboratory of the University of Perugia, Italy. From June 2009 to June 2012, he was a Postdoctoral Researcher at the Electromagnetism and Circuits Theory Department, UPM. From 2012 to 2014, he was at the Swiss Federal Institute of Technology in Lausanne (EPFL), Switzerland, as a Marie-Curie Fellow. He was at the Foundation for Research on Information Technologies in Society (IT'IS Foundation), Zurich, Switzerland, from January 2015 to September 2017, as an Electromagnetic (EM), Dosimetry, and Antenna Researcher. Since October 2017, he has been with the Information Processing and Telecommunications Center, UPM, where he is currently an Associate Professor.

• • •